



HAL
open science

Collisional-Radiative modeling and radiative emission of tungsten in tokamak plasmas in the temperature range [800-5000] eV

M. Boumendjel, C. Desgranges, R. Guirlet, Olivier Peyrusse

► **To cite this version:**

M. Boumendjel, C. Desgranges, R. Guirlet, Olivier Peyrusse. Collisional-Radiative modeling and radiative emission of tungsten in tokamak plasmas in the temperature range [800-5000] eV. *Physics of Plasmas*, 2023, 30 (9), 10.1063/5.0160913 . hal-04219897

HAL Id: hal-04219897

<https://amu.hal.science/hal-04219897v1>

Submitted on 28 Sep 2023

HAL is a multi-disciplinary open access archive for the deposit and dissemination of scientific research documents, whether they are published or not. The documents may come from teaching and research institutions in France or abroad, or from public or private research centers.

L'archive ouverte pluridisciplinaire **HAL**, est destinée au dépôt et à la diffusion de documents scientifiques de niveau recherche, publiés ou non, émanant des établissements d'enseignement et de recherche français ou étrangers, des laboratoires publics ou privés.

This is the author's peer reviewed, accepted manuscript. However, the online version of record will be different from this version once it has been copyedited and typeset.

PLEASE CITE THIS ARTICLE AS DOI: 10.1063/5.0160913

Collisional-Radiative modeling and radiative emission of tungsten in tokamak plasmas in the temperature range [800-5000] eV

M.Y. Boumendjel, C. Desgranges, R. Guirlet,¹ the West Team,^{1, a)} and O. Peyrusse²

¹⁾*CEA, IRFM, F-13108 St Paul-lez-Durance, France*

²⁾*Aix-Marseille Université, CNRS, Laboratoire LP3, UMR7341, 13288 Marseille, France*

(*Electronic mail: olivier.peyrusse@univ-amu.fr)

(Dated: 30 August 2023)

We present new collisional-modeling calculations of tungsten plasmas at electron density of about $5 \cdot 10^{13} \text{ cm}^{-3}$ and for electron temperatures in the range 0.8 to 5 keV. These conditions are relevant to current tokamaks. In this temperature range, the modeling of the ionization balance and of spectra is a long standing problem. Addressing this problem is also useful for plasmas that will be produced in the future tokamak ITER. In particular, we discuss the problem of ensuring completeness of the list of configurations included in the calculations. We also discuss comparisons of experimental measurements in the EUV range performed in the WEST tokamak with synthesized spectra based on the use of the unresolved transition array and of the spin-orbit split array formalisms. While this work does not rely on a precise identification of detailed lines, modeled spectra display emission features that looks quite similar to the experimental spectra. A conclusion is that standard calculation methods used for the evaluation of the configuration average collisional and radiative rates, are fine provided that a convenient list of configurations is used in the calculations.

^{a)}<https://irfm.cea.fr/en/west/WESTteam/>

I. INTRODUCTION

The ITER tokamak is an essential milestone in research on fusion as the energy of the future: it will be the first experimental device of sufficient size to maintain a plasma in thermonuclear combustion. Many of its plasma-facing components will be made of tungsten. This choice was motivated by its high-energy threshold of sputtering, low sputtering yield, high-redeposition efficiency, low tritium retention capacity and in addition, its excellent thermal properties.

The first two large-size tokamaks which were subsequently equipped with tungsten walls, ASDEX-Upgrade (AUG) and JET, have shown that in some experiments, tungsten accumulates in the centre of the plasma.^{1,2} The radiation then increases and can become uncontrollable, which leads to a sudden recombination of the plasma (disruption). Solutions to this problem involve either the control of the W sources from the walls or that of transport in the confined plasma³ (and preferably both). W sources on tokamak walls and transport in the poor confinement region (the so-called scrape-off layer) have been studied by means of modelling⁴ but measurements about W ions in this fairly cold region (below a few 100s eV) are difficult and scarce (see e.g. Ref. 5). W transport in the confined plasma (up to a few keV) benefits from more measurements, especially in the VUV and EUV domains, but the huge number of spectral features and their complex shape makes their identification difficult. One of the reasons of the latter difficulty is the lack of consensus of the atomic models aiming, in particular, at the determination of the ionisation balance (IB), which is the key to a realistic modelling of the W spectroscopic properties.

From the atomic physics and plasma spectroscopy point of view, it should be remembered that ionisation balance (IB), i.e. the fractional abundance of the different charge states, is the most important property for describing the plasma state. From this IB depend both the radiative energy losses and the emissivity necessary for spectroscopy diagnostics. Tokamak plasmas are extremely dilute media for which the energy distribution of the ionic states of the plasma is very far from thermodynamic equilibrium. For light elements, it is close to what is called the *coronal* equilibrium. Ionization is then essentially the result of a balance between collisional ionization and radiative recombination. For a high Z element such as tungsten, where the ions contain a lot of bound electrons in several closed inner shells, the dominant pathway to ionization is usually excitation (or capture) to autoionizing resonance states. Therefore, autoionization/resonant capture processes and the associated radiative cascades become extremely important and make the previous quasi-coronal description even more complex. In a diluted plasma, the problem remains open

This is the author's peer reviewed, accepted manuscript. However, the online version of record will be different from this version once it has been copyedited and typeset.

PLEASE CITE THIS ARTICLE AS DOI: 10.1063/1.50160913

because of many uncertainties concerning the quality of autoionization rates and concerning the *completeness* (i.e. the atomic levels to be taken into account) necessary for the population kinetics. Furthermore, spectral emission of these heavy elements is characterized by many overlapping features containing a huge number of lines making it necessary to use global statistical methods to analyse or model them. Research in this field is related to the physics of complex atoms where one faces the problem of dealing with a very large number of atomic levels. Thus, for the calculation of population kinetics and emissivity, proper averaging of levels, rates and lines, can hardly be avoided.

As mentioned above, models for calculating ionization distribution and spectral emission encounter difficulties when dealing with heavy elements. This work addresses some of these issues in the specific case of tungsten in tokamak plasmas. Temperatures considered are in the range 0.8 - 5 keV characterizing existing or past tokamaks. Also, we do not focus on the relatively cold ITER divertor plasmas of temperatures in the range 25 - 150 eV and of higher density. We report here calculations of ionic abundances and emission spectra of tungsten for the interpretation of spectroscopic measurements. These calculations are based on configuration average (CA) mode and make use of the *Unresolved Transition Arrays* (UTA) and of the *Spin-Orbit-Split Arrays* (SOSA) theories, and use a proper configuration averaging of levels, rates and spectral structures as reviewed in Ref. 6. These methods have been applied with a noticeable success to dense plasmas, e.g. hot laser-produced plasmas (see for instance Ref. 7). In the present tokamak context, we did not make any adjustment to the recombination rates to reconcile the results with measurements as done in Ref. 8 with another approach (this point is discussed below). These calculations are compared with spectra observed on the WEST tokamak. This device benefits from radiation measurement systems not available on AUG and JET, namely an optimized far-UV (EUV) spectrometer with a moving line of sight and a soft X-ray measurement system with energy resolution.

This work takes place in an effort aiming at determining the density of tungsten throughout the plasma. Ultimately, the results will be compared to theoretical transport models, in particular transport due to turbulence, in order to understand how to avoid tungsten accumulation in the plasma.

II. ATOMIC MODEL FOR TUNGSTEN IN TOKAMAK CONDITIONS

Many studies have already been published concerning the ions of tungsten (energy levels, spectral lines). A review can be found in Ref. 9. In particular, devices smaller than tokamaks such as electron-beam ion traps (EBIT) allowed spectral measurements of specific ions of tungsten from the medium to the rather high charge-state range.^{10–13} Concerning the kinetics, and more specifically, the calculation of the ionization balance (IB) of W, various models have been proposed, e.g. ADPAK.¹⁴ Later, a modification of ADPAK was proposed for a better matching with experimental results.¹⁵ Still later, Loch *et al* proposed improved ionization rates (taking into account autoionization/resonant capture)¹⁶ but, even with this improved version of ADPAK, Pütterich *et al* found discrepancies between predictions and experiments.⁸ Hence they proposed an *ad hoc* modification of recombination rates of ADPAK⁸ which is now adopted in the OPEN-ADAS data base.¹⁷ A conclusion of these studies is that it is crucial to understand the complex W population kinetics especially in the range 0.8 - 3 keV where the most abundant ions have electrons in open N-shell configurations.

Population kinetics calculations or *collisional-radiative modeling* consist in obtaining the population set $\{N_i^{(z)}\}$ for atomic levels i in all charge states z . This set is obtained by solving the system

$$\frac{dN_i^{(z)}}{dt} = \sum_{z'} \sum_j N_j^{(z')} T(z', j \rightarrow z, i) - \sum_{z'} \sum_j N_i^{(z)} T(z, i \rightarrow z', j) \quad (1)$$

where $T(z', j \rightarrow z, i)$ and $T(z, i \rightarrow z', j)$ are the global (i.e. summed over various collisional and radiative processes) populating rates, and the global depopulating rates of level i in the ionic species z , respectively. One notices here that *steady-state* solution corresponds to $\frac{dN_i^{(z)}}{dt} = 0$. The main difficulty in collisional-radiative modeling, is well known: there is literally an infinite number of levels in the isolated ions. Fortunately, the microscopic processes at work in plasmas with maxwellian electrons avoid us to consider most of the possible highly and multiply excited levels. Also, the plasma continuum lowering effect helps to reduce the number of levels by cutting off highly-excited levels. But still, there are no obvious rules to select the important levels to be taken into account for a given set of parameters temperature-density. This is the problem of *completeness* of levels in collisional-radiative models (CRM) (for a discussion concerning this problem, see for instance Ref. 18) with the observed trend that models with an insufficient number of levels tend to overpredict ionization. At the basic atomic level, one has to list the important *fine-structure*

(FS) levels or, for the sake of simplification, just the configurations spawning these levels, this is the sense of configuration average (CA) calculations where one considers only the set $\{N_c^{(z)}\}$ (with $N_c^{(z)} = \sum_{i \in c} N_i^{(z)}$) and where instead of (1), one solves the reduced system

$$\frac{dN_c^{(z)}}{dt} = \sum_{z'} \sum_{c'} N_{c'}^{(z')} T(z', c' \rightarrow z, c) - \sum_{z'} \sum_{c'} N_c^{(z)} T(z, c \rightarrow z', c') \quad (2)$$

in which $T(z, c \rightarrow z', c') = \sum_{i \in c} \sum_{j \in c'} \frac{g_i}{g_c} T(z, i \rightarrow z', j)$ is a configuration average rate. g_i is the statistical weight of FS level i and g_c is the statistical weight of configuration c . It turns out that FS versus CA calculations are only possible in light elements, i.e. those for which the number of FS levels remains tractable. Between CA and FS calculations, comparisons may show some disagreements due to the existence of metastable levels (which are naturally taken into account with a FS description). Obviously, CA models have also a lower fidelity at the spectroscopic level but their advantage is that completeness is easier to satisfy. Indeed, the calculation of ionization balance in high-Z elements involves too many FS levels for a reliable calculation to be tractable. One must resort to a bundling of levels, i.e. to the configuration averaging (CA) mentioned above or even to the superconfiguration averaging (SCA) and/or a mix of both.¹⁹ In the latter case, it has been shown that a convergence on the average ionization (and thus on IB) can be observed when one splits gradually the superconfigurations (SC) into configurations. While this convergence is fast in high density plasmas (e.g. laser-produced plasmas), it is more difficult in lower density plasmas and may lead to an untractable number of configurations when one deals with complex many open-shell configurations such as in tokamak plasmas where tungsten is present as an impurity and for temperatures of about 1-2 keV. The notion of consistent effective temperature inside each SC, i.e. assuming a Boltzmann-like distribution of configuration populations in each SC, may be an alternative.^{20,21} However, as discussed in Ref. 6 (p.278) a breakdown of effective temperatures and of the CRM with SCs occurs at electron densities typically below 10^{17} cm^{-3} . Reasons invoked are that, for these "low" densities, (i) populations of excited configurations become very weak (which means that an overwhelming majority of ions resides in ground state), (ii) a SC represents too large an energy range of levels (even though it is a convenient way to include many configurations), (iii) there are no more effective SC temperatures. An additional remark concerning high-Z complex ions can be made: above the first ionization threshold of an ion of charge z , there are many multiply-excited electron states that form resonances for resonant capture of free electrons. These states are connected via autoionization with the ion of charge $z + 1$. It turns out that these resonances affect profoundly the IB.

For all of those reasons, we decided to adopt a specific strategy for approaching the completeness adapted to the W-contaminated plasmas found in tokamaks. First of all, we gave up the idea of superconfiguration for these calculations. Instead we make a configuration selection by a specific *promotional strategy* from the ground configuration of each ion. Thus, we proceed in 4 steps summarized as follows:

- step 0 (label S_0), we take the ground configuration and retain one-electron excitation from the last occupied subshell.
- step 1 (label S_1), one considers the excitation of a second electron from the last occupied subshell (only if it contains at least 2 electrons in the ground configuration),
- step 2 (label S_2), still from the ground configuration, one considers the excitation of one electron from the second last occupied subshell,
- step 3 (label S_3), from configurations resulting from S_0 (with the exception of the ground one), one considers the excitation of one-electron from the second last occupied subshell to the outer subshells.

These different steps are best explained taking the example of the Zr-like ion (40 electrons). Here, for shortening the notations, $(3)^{18}$ means $3s^2 3p^6 3d^{10}$ while for instance $(5-10)^2$ represents all the permutations of 2 electrons in the different subshells belonging to shells $n=5$ to $n=10$.

S_0 gives,

$$\begin{aligned} &(1)^2 (2)^8 (3)^{18} 4s^2 4p^6 4d^4 \text{ (ground configuration),} \\ &(1)^2 (2)^8 (3)^{18} 4s^2 4p^6 4d^3 4f, \\ &(1)^2 (2)^8 (3)^{18} 4s^2 4p^6 4d^3 (5-10)^1, \end{aligned}$$

i.e. 47 configurations.

S_1 gives,

$$\begin{aligned} &(1)^2 (2)^8 (3)^{18} 4s^2 4p^6 4d^2 4f^2, \\ &(1)^2 (2)^8 (3)^{18} 4s^2 4p^6 4d^2 4f (5-10)^1, \\ &(1)^2 (2)^8 (3)^{18} 4s^2 4p^6 4d^2 (5-10)^2, \end{aligned}$$

i.e. 1081 configurations.

S_2 gives,

$$\begin{aligned} &(1)^2 (2)^8 (3)^{18} 4s^2 4p^5 4d^5, \\ &(1)^2 (2)^8 (3)^{18} 4s^2 4p^5 4d^4 4f, \\ &(1)^2 (2)^8 (3)^{18} 4s^2 4p^5 4d^4 (5-10)^1, \end{aligned}$$

i.e. 47 configurations.

S_3 gives,

$$(1)^2 (2)^8 (3)^{18} 4s^2 4p^5 4d^3 4f^2,$$

$$(1)^2 (2)^8 (3)^{18} 4s^2 4p^5 4d^3 4f (5-10)^1,$$

$$(1)^2 (2)^8 (3)^{18} 4s^2 4p^5 4d^3 (5-10)^2,$$

i.e. 1081 configurations.

This results in 2256 configurations in this ion stage, which remains very reasonable since a typical calculation with about 20 ion stages centered around the mean ionization leads to about 40,000 - 50,000 rate equations of kind (2). A more concise and visual presentation of steps S_0 - S_3 is given in Fig. 1. As we will see, the addition of configurations obtained in step 3 has a dramatic effect on the IB. Of course we have no guarantee that this method provides a fully *converged* list of configurations. However, the comparison with experimental spectra shown in the Sect. 4 led us to conclude tentatively that the list generated in this way, is reasonably well converged.

Our CA calculations started with a computation of the configuration energies based on the Hartree-Fock-Slater (HFS) method, with an exchange potential of the form (in a.u.) $v_x = -3\alpha_x(\frac{3}{8\pi})^{1/3}\rho^{1/3}$ where for W, the parameter α_x was set to 0.78²² (instead of the standard value of 2/3). In these calculations, mass-velocity and Darwin relativistic corrections have been accounted for. Then, rates or cross sections for the various processes (E1 and E2 radiative transition, electron-impact excitation, electron-impact ionization, photoionization, and autoionization) were computed according to the methods discussed in Ref. 23. These data are used to build a standard system of coupled collisional-radiative equations, solved in the steady-state regime.

III. RESULTS OF COLLISIONAL-RADIATIVE MODELING

We first present in Figure 2 the average ionization $\bar{Z} = \sum_{c \in z} z N_c^{(z)} / \sum_{c \in z} N_c^{(z)}$ of tungsten in the electron temperature range 0.8 - 5 keV as calculated with the four lists of configurations: S_0 , S_0+S_1 , $S_0+S_1+S_2$ and $S_0+S_1+S_2+S_3$ respectively. We see that below 2 keV, \bar{Z} undergoes a strong variation and that the addition of configurations issued from S_3 has a dramatic impact on this average ionization. This means that these configurations open important channels for resonant captures. It turns out that these last calculations performed with a modest number of configurations (of the order of 50,000 on the whole) lie much closer to ionization inferred from experiments⁸ than

This is the author's peer reviewed, accepted manuscript. However, the online version of record will be different from this version once it has been copyedited and typeset.

PLEASE CITE THIS ARTICLE AS DOI: 10.1063/1.50160913

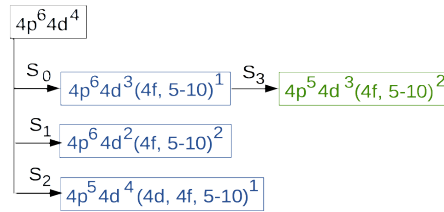


FIG. 1. Schematic diagram of the promotional strategy exemplified on ion W^{34+} . Ground configuration is here $(1)^2 (2)^8 (3)^{18} 4s^2 4p^6 4d^4$. S_0 : one-electron excitation from the last occupied subshell (here 4d) S_1 : excitation of a second electron from the last occupied subshell (here 4d). S_2 : excitation of one electron from the second last occupied subshell (here 4p) S_3 : after S_0 , excitation of one-electron from the second last occupied subshell.

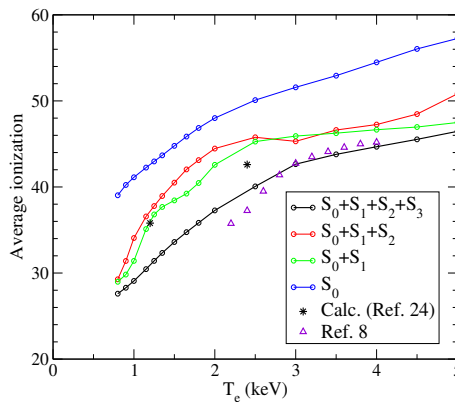


FIG. 2. Average ionization as a function of temperature at electron density of $5 \cdot 10^{13} \text{ cm}^{-3}$, for the different lists of configurations discussed in the text. The two calculation points of Ref. 24 are also reported as well as semi-empirical results of Ref. 8.

calculations performed with a much larger number of configurations²⁴ and without any artificial factor introduced on the recombination rates. While calculations of Ref. 24 considered a very large number of configurations mostly spawned from large SCs (although with necessary restrictions), it turns out that many configurations spawned from the complexes $(3)^{18} (4)^{10} (7-10)^2$ (the specific

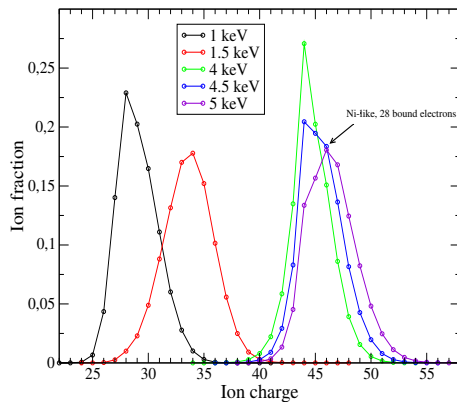


FIG. 3. Ionization distribution of tungsten at five temperatures and electron density of $5 \cdot 10^{13} \text{ cm}^{-3}$.

Zr-like ion is kept as example) are not taken into account in these calculations. With regard to our choice in S_1 and S_3 , we thus identified here important configurations which have to be considered for an accurate completeness of configurations in low density high-Z plasmas. In particular, the promotion of 2 electrons from 4p, 4d, 4f to all subshells with $n = 5-10$ seems to play an important role. Hereafter, all calculations are performed from lists $S_0+S_1+S_2+S_3$.

A comparison of the ionization distribution at five temperatures in the range 1 keV to 5 keV (Figure 3), is also instructive. While they are obviously shifted, the last three ones are close to each other. This is a clear illustration of the shell-closure effect where ionization tends to favor closed-shell ions. Moreover, at 4 keV, the mean calculated ion charge is about 44 while available experimental data obtained in an impurity accumulation mode (Ref. 8), suggests an optimal temperature of 3.5 keV for this ion charge. However, this difference remains compatible with the uncertainty associated with the temperature measurement reported in Ref. 8.

IV. EMISSION SPECTRA - COMPARISON WITH EXPERIMENTS

A. Calculation of tungsten radiative emission

Using the previously calculated population distribution of configurations, spectral modeling has been realized using the UTA/SOSA formalism (see Refs. 25 and 26 and references therein). For each couple of configurations (c, c') connected by radiative emission (i.e. forming a *Transition*

Array), the contribution to the emissivity reads in the UTA limit

$$j_{cc'}(\nu) = \frac{h\tilde{\nu}}{4\pi} A_{cc'} N_c^{(z)} \phi_{cc'}(\nu) \quad (3)$$

and this formalism allows to calculate properly the average position $\tilde{\nu}$ and width characterizing the (gaussian) profile $\phi_{cc'}$ of each array. In (3), $A_{cc'}$ is the configuration average spontaneous emission rate. It is also possible to include relaxation,²⁷ i.e. the fact that the potential of the lower configuration is not strictly identical to the potential of the upper configuration in the radiative electron jump. Considering the relativistic configurations spawned by the previous non-relativistic ones, spin-orbit interaction may split the UTA into 2-3 peaks called SOSAs. An approximate treatment of configuration interaction between the two most intense SOSA peaks is possible.²⁸⁻³⁰ At this step, the treatment of transitions between very simple pairs of configurations where a statistical approach does not make sense, deserves comments. Taking the example of the transitions $4d^9 4f - 4d^{10}$ in the Pd-like ion (46 bound electrons), if the SOSA formalism splits properly the UTA into the right number of lines (i.e. three), the position and intensity of these lines are not correct. The main reason is that an underlying assumption of a statistical treatment is the statistical population of levels inside a configuration, i.e. according to their statistical weights. In fact, in low density plasmas, population of a level i in an upper weakly degenerated configuration rather results from a simple balance between collisional excitation from the ground level of the lower configuration (rate C_{1i}) and radiative deexcitation toward this level (rate A_{i1}), i.e. one has $N_i A_{i1} = C_{1i} N_1$. As a consequence, it is more appropriate to build the emissivity with an upper population thus defined and use a lorentzian profile for each of the 3 lines. In this paper, we applied this procedure for each pair of configurations where the lowest one is not degenerated. The rate A_{i1} we used results from an atomic structure calculation while the rate C_{1i} makes use of a cross section calculated at the distorted wave (DW) approximation. In the calculated spectral emissivities presented below (Figs 3-4) and which assume an infinite resolution, these lines correspond to the most prominent and very narrow peaks. These lines are likely to be strongly affected by instrumental broadening.

It is interesting to look at the emission as calculated on a large spectral range. Figure 4 displays the W emission calculated for $T_e = 1000$ eV and 1500 eV, respectively. These spectra (of infinite resolution) correspond to a pure tungsten plasma.

One observes bright and prominent emission features for photon energies between 180 eV and 350 eV (35 - 70 Å in wavelength). These structures contain a very large number of overlapping lines and form what is called the quasi-continuum (QC) emission of W in this temperature range.

This is the author's peer reviewed, accepted manuscript. However, the online version of record will be different from this version once it has been copyedited and typeset.

PLEASE CITE THIS ARTICLE AS DOI: 10.1063/1.50160913

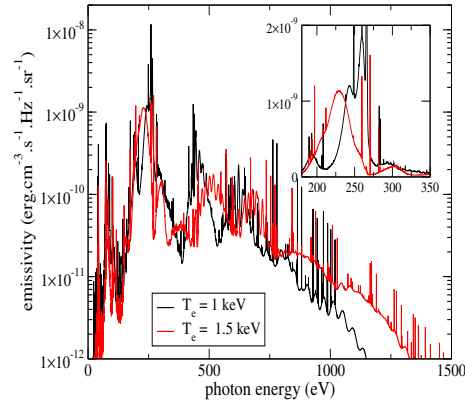


FIG. 4. Calculated tungsten emission spectra on a large spectral range for $T_e = 1$ keV (black) and $T_e = 1.5$ keV (red), respectively. Electron density is $n_e = 5 \cdot 10^{13} \text{ cm}^{-3}$. The inset is a linear scale zoom of the emission in the interval 180 - 350 eV of maximum emission.

In addition, on the top of the QC, isolated lines are superimposed. In Fig. 4, one sees that this QC emission is particularly distinguishable which explains why it has been investigated on various devices. Also one notices that this QC is of importance concerning the total radiated power. Thus, hot tungsten plasma spectroscopy started at ORMAK.³¹ In particular, what was observed is unresolved, wide band-like structures between 40 and 70 Å. This was later confirmed at TEXT³² and at ASDEX Upgrade.¹⁵ These structures, corresponding to a very large number of superimposed lines originating from transitions of the type $4d^{10} 4f^n - 4d^9 4f^{n+1}$, $4d^{10} 4f^n - 4d^9 4f^n 5p$ and $4d^{10} 4f^n - 4d^{10} 4f^{n-1} 5\ell$ ($\ell = d, g$) in ions W^{24+} to W^{35+} , were interpreted for the first time in terms of unresolved transition arrays (UTAs).³²

One can notice that this specific EUV QC emission was also observed in experiments carried out in the LHD device in the electron temperature range 0.6 - 1.3 keV.³³ In these experiments, the tungsten was intentionally injected in the device in order to observe its emission spectrum.

B. Main EUV spectral features

We now examine the emission spectrum of W in this QC range of 15 - 70 Å. We first present in Fig. 5, the calculated emission for a few temperatures in the range [800-1350] eV. These are purely

This is the author's peer reviewed, accepted manuscript. However, the online version of record will be different from this version once it has been copyedited and typeset.

PLEASE CITE THIS ARTICLE AS DOI: 10.1063/1.50160913

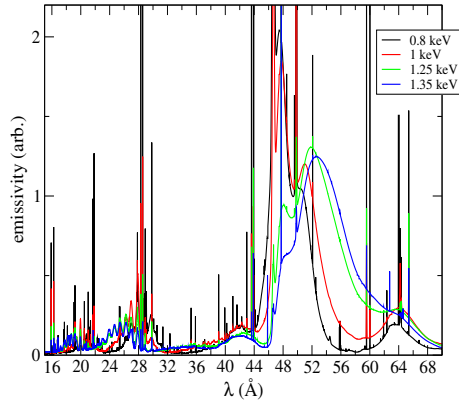


FIG. 5. Calculated tungsten EUV spectra for four temperatures in the range [800 - 1350] eV (infinite resolution).

theoretical spectra calculated assuming an infinite resolution. In this temperature range, EUV UTA emission comes from ionization stages from Ag-like W^{27+} to Br-like W^{39+} . One notices a broad structure in the interval [45 - 70] Å, which does not move clearly with temperature (at least in this temperature range) while its shape is changing. This interval consists of 4f-4d transitions in the afore-mentioned ions both in the main broad feature [45 - 55] Å, and in the secondary feature [55 - 70] Å. The latter contains also 4d-4p, 4p-4s, 5d-4f, 6s-5p, and 6p-5d transitions. This secondary feature seems to move toward shorter wavelengths when T_e increases. One remarks here that Pütterich *et al*⁸ tried to reproduce this feature with a detailed fine-structure approach but they did not succeed. The interval [20 - 35] Å is also interesting as it contains features which clearly moves toward shorter wavelengths when T_e increases. This interval consists of 5p-5s, 5p-4d, 5g-4f, 6d-4f and 6g-4f transitions. Around 42 Å, there is a broad feature whose intensity increases with T_e . It consists of 4d-4p, 5d-4f, 6p-5s and 6d-5p transitions. For higher temperatures, the feature [45 - 55] Å, corresponds to emission of ions W^{35+} to W^{41+} . Last, one notices here that the range of 4-4 ($\Delta n = 0$) transitions is likely to be strongly affected by the configuration interaction (CI) effect which modifies energies and oscillator strengths.

C. Comparison with experiments

In tokamak plasmas, the domain of interest for spectroscopic diagnostics is the EUV range as most emission of highly ionized heavy impurities, tungsten in particular, lies in the 10 - 400 Å wavelength region. Spectra measured with sufficiently high accuracy and resolution can provide detailed information on the impurity atomic structure and their concentration inside the plasma.^{15,34}

On the WEST tokamak, the EUV spectra are recorded with a high-resolution 2-m grazing incidence Schwob-Fraenkel spectrometer³⁵ named SIR. It is equipped with a 600 grooves mm⁻¹ concave grating, and two mobile detector assemblies which are used to scan the wavelength domain along the Rowland circle. Each one is made of a pair of multichannel plates (MCPs) followed with a phosphor screen which converts the photoelectrons into visible photons. These photons are then detected by a 1340x1300 pixels CCD camera. By moving the two MCPs along the Rowland circle, the spectrometer is capable of covering a large wavelength band from 15 to 340 Å with a high spectral resolution (FWHM of about 0.18 Å at 25 Å and 0.23 Å at 120 Å). The typical time resolution (i.e. the best compromise between time resolution and a satisfactory signal-to-noise ratio) is 15 ms.

The SIR has been calibrated in absolute units of brightness (photons m⁻² s⁻¹ sr⁻¹).³⁶ The calibration has been performed using Kα lines of six different elements in the wavelength domain 10-113 Å and a relative calibration of the domain above 113 Å has been done using spectral line brightness ratios calculated by a collisional radiative model. The global calibration uncertainty was estimated to be 20% below 113 Å, and up to 40% above. The spectrometer is mounted on a mobile frame connected to an electric jack controlled by a stepper motor. It can scan vertically the lower plasma half at a frequency of 0.5 Hz, covering the region between the magnetic axis and the lower divertor.

A series of experiments have been conducted on WEST where W spectra have been recorded with the SIR spectrometer. To obtain the measurements presented in the following, the spectrometer was used with a fixed line of sight during two typical discharges WEST#54723 and WEST#55522 i.e. the spectrometer line of sight crosses almost horizontally the magnetic axis during the discharges as illustrated in Figure 6.

The main parameters of these two typical discharges are shown in Figure 7 (WEST#54723) and Figure 8 (WEST#55522), respectively. The first discharge WEST#54723, shown in Figure

This is the author's peer reviewed, accepted manuscript. However, the online version of record will be different from this version once it has been copyedited and typeset.

PLEASE CITE THIS ARTICLE AS DOI: 10.1063/1.50160913

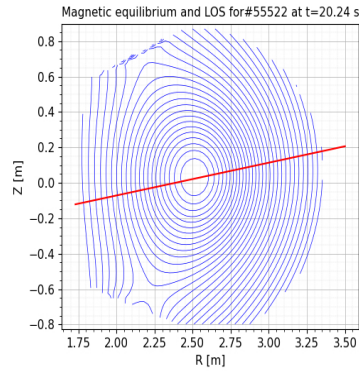


FIG. 6. The magnetic equilibrium (WEST#55522 case) with the spectrometer line of sight (LOS). The spectroscopic measurements are integrated along the line of sight, and the plasma parameters (density and temperature in particular) are spatially uniform on the flux surfaces.

7, starts with ohmic heating and then is maintained stable from 4.5 s to 9.5 s by a small amount of lower hybrid (LH) wave power. The plasma current is about 0.5 MA, and the central temperature and density reach about 1.1 keV and $4.1 \cdot 10^{19} \text{ m}^{-3}$, respectively. The second discharge WEST#55522 shown in Figure 8, is sustained by continuous LH heating. The plasma parameters, central temperature and density, are maintained stable from 8 s to 25 s, with values of about 3.9 keV and $3.7 \cdot 10^{19} \text{ m}^{-3}$, respectively. The electron density as a function of the radial coordinate is obtained by tomographic inversion of measurements with the help of a far IR interferometer and by using a hyperbolic tangent fit.³⁷ The electron temperature measurements were obtained by means of an electron cyclotron emission (ECE) radiometer. The uncertainties in the temperature profile determination may reach 15-20% in the plasma core and 40% close to the plasma edge ($r > 0.35\text{-}0.4 \text{ m}$). In fact, the temperature measurements by the ECE radiometer are usually not valid beyond $r = 0.6 \text{ m}$ because of the plasma low density and the presence of suprathermal electrons.³⁸

In these discharges, tungsten is an intrinsic impurity, originating from the tungsten divertor plates and the other W surfaces facing the plasma. The EUV spectra, recorded in the wavelength region from 40 to 70 Å and displayed in Figs 10-11, are averaged over 0.5 s to improve the signal-to-noise ratio. More specifically, the spectrum corresponding to WEST#54723 is averaged over the interval 7.5-8 s, while the spectrum corresponding to WEST#55522 is averaged over the interval

This is the author's peer reviewed, accepted manuscript. However, the online version of record will be different from this version once it has been copyedited and typeset.

PLEASE CITE THIS ARTICLE AS DOI: 10.1063/1.50160913

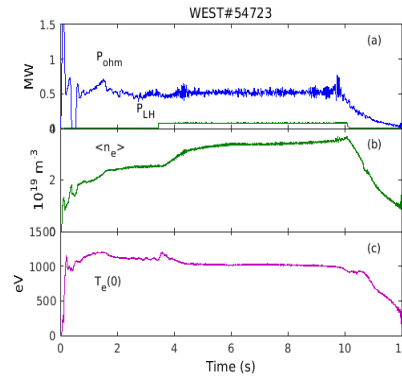


FIG. 7. Discharge WEST#54723 : (a) Time behavior of the power injected in the plasma, ohmic heating (ohm) and lower hybrid (LH) heating, (b) electron density and (c) electron temperature at the center of the plasma.

20-20.5 s. The corresponding density and temperature profiles are shown in Figure 9. We note that for WEST#55522, the temperature range explored by the spectrometer line of sight is substantially broader than that of WEST#54723. In the former case (WEST#55522), the radial distribution of both n_e and T_e (see Fig. 9) is expected to play an important role in the measured EUV radiation. In other words, the sum over different emitting zones along the line of sight has to be invoked here.

Figure 10 (top figure) shows the EUV spectrum corresponding to WEST#54723, as measured using the spectrometer SIR in the range $[35 - 70] \text{ \AA}$ (and averaged in the time interval 7.5-8 s, as mentioned above). Figure 10 also shows synthesized spectra using the methods mentioned above, for different temperatures around the maximum temperature of the plasma (see Fig. 9). The calculated spectra have been convolved with a gaussian of FWHM 0.2 \AA . We did not attempt to make a proper quantitative comparison. We restrict our comments to the most obvious features of the spectra which are extremely complex and for which a line by line account of all transitions is impossible. We remind that our calculations are Hartree-Fock-Slater calculations, not fully relativistic but based on a properly implemented UTA/SOSA description of the spectral emission. As discussed in paragraph 4.1, this statistical approach cannot provide an accurate description when the SOSAs contain a single line (the statistical variance of those SOSAs is 0). This is the case for transitions $4d^9 4f - 4d^{10}$ in the Pd-like ion or for transitions $4p^5 4d - 4p^6$ in the Kr-like

This is the author's peer reviewed, accepted manuscript. However, the online version of record will be different from this version once it has been copyedited and typeset.

PLEASE CITE THIS ARTICLE AS DOI: 10.1063/1.50160913

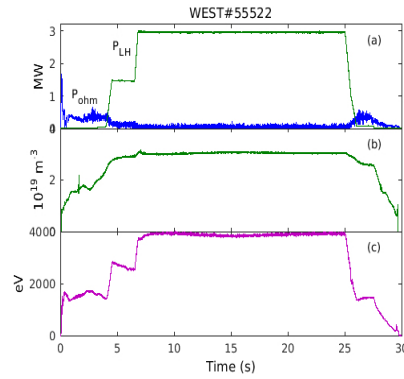


FIG. 8. Discharge WEST#55522 : (a) Time behavior of the power injected in the plasma, ohmic heating (ohm) and lower hybrid (LH) heating, (b) electron density and (c) electron temperature at the center of the plasma.

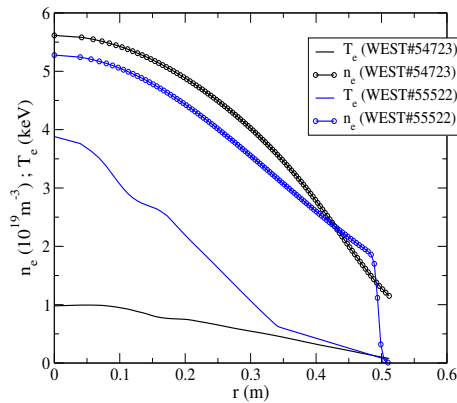


FIG. 9. Radial profiles of n_e , T_e at $t = 7.5$ s, for WEST#54723 (black curves) and at $t = 20$ s for WEST#55522 (blue curves), respectively.

ion. Another issue is that transitions $\Delta n = 0$, with $n = 4$ may be strongly affected by configuration interaction (CI) effects which change oscillator strengths and line positions. In particular, the mixing between configurations $4p^6 4d^{m-1}4f$ and $4p^5 4d^{m+1}$, $m = 1 - 9$, i.e. in ions W^{37+} to W^{29+} turns out to be important.¹⁰ Despite these limitations, the global features of the measured spectrum

This is the author's peer reviewed, accepted manuscript. However, the online version of record will be different from this version once it has been copyedited and typeset.

PLEASE CITE THIS ARTICLE AS DOI: 10.1063/1.50160913

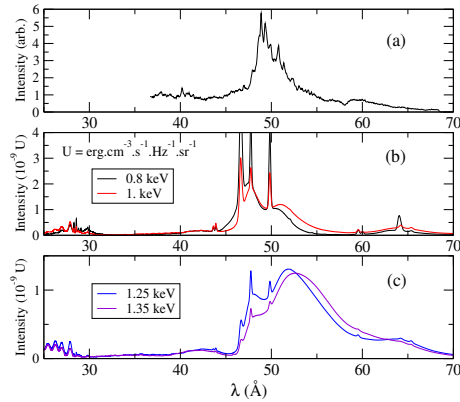


FIG. 10. (a) EUV spectrum averaged between 19 and 20 s for the discharge corresponding to WEST#54723. (b, c) Calculated EUV spectra with a UTA/SOSA description, for different temperature between 0.8 and 1.35 keV.

are rather well reproduced by the calculation given the uncertainty of 15-20% on the measured temperature. Calculated spectra suggest here a temperature of about 1 to 1.2 keV. The wavelength interval in which lies the QC is modeled with a very satisfactory accuracy. Note in particular that the steep rise of the main structure's left wing measured at 46-48 Å is well reproduced by the model. The shape of this structure is also well reproduced: a very prominent, broad peak around 50 Å which the model reveals to be the sum of two broad features and the weak feature around 60 Å which is modeled at a slightly higher wavelength. The structure modeled at 40-45 Å might correspond to the left foot of the main feature measured in the 45-48 Å interval. Below 30 Å, the modeled spectrum is reminiscent of the 'sawtooth' aspect of measurements in WEST and other devices (see for instance Ref. 33). We note that for a temperature of 1 keV, the calculated average ionization is $\langle Z \rangle = 29.08$ and the emission is mainly due to charge states W^{27+} to W^{31+} (see Figure 3). In the modeled spectra of Figure 10, prominent narrow peaks in the interval 46-50 Å correspond to the contribution of the W^{28+} ion (46 bound electrons), i.e. to lines $4d^9 4f - 4d^{10}$ and also to lines $4f - 4d$ in slightly higher ionization stages. For these lines, a precise position cannot be expected with the present formalism which ignores configuration interaction.

Figure 11 (a) shows the EUV spectrum corresponding to WEST#55522, as measured in the same conditions as case WEST#54723. Because of the strong radial variation of temperature

This is the author's peer reviewed, accepted manuscript. However, the online version of record will be different from this version once it has been copyedited and typeset.

PLEASE CITE THIS ARTICLE AS DOI: 10.1063/1.50160913

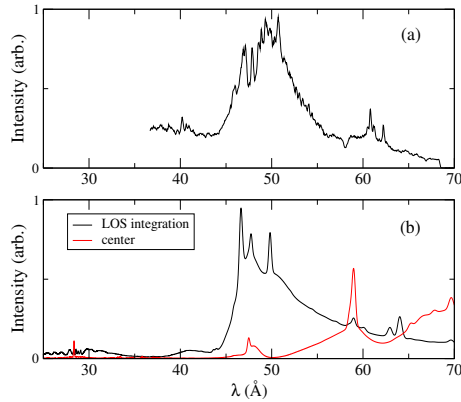


FIG. 11. (a) EUV spectrum averaged between 20 and 20.5 s for the discharge corresponding to WEST#55522. (b) Calculated EUV spectra with a UTA/SOSA description. Here the calculation corresponds to emission integrated over ten (T_e , N_e) zones taken from the gradients of Figure 8 (Line Of Sight integration). Red curve is the emission corresponding to the central zone.

and density in this case (see Fig. 9), one expects the emissivity to be strongly inhomogeneous along the line of sight of the spectrometer. Figure 11 (b) displays the synthesized spectrum (LOS integration) resulting from adding ten consecutive emitting zones taken along the gradients (T_e , n_e) of Figure 8 (WEST#55522). For information, the emissivity of the central zone is also displayed (red curve). Here also, global features of the spectrum are reproduced. In this hot plasma, both the measured and the modeled spectra exhibit a more intense feature around 60 Å with respect to the main feature. The brightness ratio of the two features is also well reproduced. Again, the feature modeled at 40-45 Å is not visible in the measurements, possibly because its actual wavelength is slightly larger (45-48 Å) than modeled. We note also that the main feature becomes broader, both in the model and the measurements. At about 4 keV (central zone of the plasma) the calculated average ionization lies between 44 and 45 so that the emission is mainly due to ion stages W^{43+} to W^{46+} (see Figure 3). In the modeled spectra of Figure 11, prominent narrow peaks around 60 Å correspond to the contribution of the W^{44+} ion (30 bound electrons) and W^{45+} ion (29 bound electrons) i.e. to single lines of the kind 4p - 4s. Again for these lines (in these ions), a precise position cannot be expected with the present formalism.

V. SUMMARY

We have developed a tungsten atomic model based on standard configuration-averaged energies and rates although calculated with proper quantum mechanical methods (i.e. not relying on any hydrogenic approach). The resulting synthetic spectra rely on a proper implementation of the UTA/SOSA theory. In a range of temperatures between 1 and about 2.5 keV, we evidenced a strong sensitivity of the ionization balance on the list of configurations included in the model. From the resulting spectra and a comparison with tungsten experimental spectra measured on the WEST tokamak, we shown that a specific choice of the configuration list allows one to capture the large complexity of highly ionized tungsten spectra, and in particular, to recover most of the features of the quasi-continuum (QC) emission. An important specificity of these calculations is that no modification of the ionization and recombination rates has to be invoked to recover or at least to approach a reasonable ionization balance.

To go beyond the UTA/SOSA approach, it could be interesting to predict emission using a mixed-unresolved-transition-array (MUTA) approach,³⁹ i.e. an approach which allows to capture more details in the emission. However this approach cannot address strong CI effects between different arrays (which is a concern for $n=4 - n=4$ transitions). Another improvement could be an artificial adjustment of energies and intensities for the simplest SOSAs (those with a zero variance), from the results of specific detailed atomic physics calculations taking into account CI.

As a last comment, this work is a prerequisite for any work aiming at characterizing tokamak plasmas by using tungsten broadband emission, for calculating line emission coefficients or more generally radiation power losses.

ACKNOWLEDGMENTS

This work has been carried out within the framework of the EUROfusion Consortium, funded by the European Union via the Euratom Research and Training Programme (Grant Agreement No 101052200 - EUROfusion). Views and opinions expressed are however those of the author(s) only and do not necessarily reflect those of the European Union or the European Commission. Neither the European Union nor the European Commission can be held responsible for them.

The authors thank Professor Jean-Louis Schwob from Jerusalem University and Professor Pierre Mandelbaum from Azrueli College of Jerusalem for helpful discussions.

REFERENCES

- ¹R. Neu, R. Dux, A. Kallenbach, T. Pütterich, M. Balden, J.C. Fuchs, A. Herrmann, C.F. Maggi, M. O'Mullane, and R. Pugno, "Tungsten: an option for divertor and main chamber plasma facing components in future fusion devices," *Nucl. Fusion* **45**, 209 (2005).
- ²T. Pütterich, R. Dux, R. Neu, M. Bernert, M. N. A. Beurskens, V. Bobkov, S. Brezinsek, C. Challis, J. W. Coenen, I. Coffey, A. Czarnecka, C. Giroud, P. Jacquet, E. Joffrin, A. Kallenbach, M. Lehnen, E. Lerche, E. de la Luna, S. Marsen, G. Matthews, M.-L. Mayoral, R. M. McDermott, A. Meigs, J. Mlynar, M. Sertoli, G. van Rooij, the ASDEX Upgrade Team, and JET EFDA Contributors, "Observations on the W-transport in the core plasma of JET and ASDEX Upgrade," *Plasma Phys. Control. Fusion* **55**, 124036 (2013).
- ³M. Valisa, L. Carraro, I. Predebon, M.E. Puiatti, C. Angioni, I. Coffey, C. Giroud, L. Lauro Taroni, B. Alper, M. Baruzzo, P. Belo daSilva, P. Buratti, L. Garzotti, D. Van Eester, E. Lerche, P. Mantica, V. Naulin, T. Tala, M. Tsalias, and JET-EFDA contributors, "Metal impurity transport control in JET H-mode plasmas with central ion cyclotron radiofrequency power injection," *Nucl. Fusion* **51**, 033002 (2011).
- ⁴H. Bufferand, P. Tamain, S. Baschetti, J. Bucalossi, G. Ciraolo, N. Fedorczak, Ph. Gendrih, F. Nespoli, F. Schwander, E. Serre, and Y. Marandet, "Three-dimensional modelling of edge multi-component plasma taking into account realistic wall geometry," *Nuclear materials and energy* **18**, 82 (2019).
- ⁵K. D. Lawson, E. Pawelec, I. H. Coffey, M. Groth, E. Litherland-Smith, A. G. Meigs, S. Scully, and JET Contributors, "Observation of low temperature VUV tungsten emission in JET divertor plasmas," *Physica Scripta* **97**, 055605 (2022).
- ⁶J. Bauche, C. Bauche-Arnoult, and O. Peyrusse, *Atomic Properties in Hot Plasmas - From Levels to Superconfigurations* (Springer, 2015).
- ⁷C. Chenais-Popovics, V. Malka, J.C. Gauthier, S. Gary, O. Peyrusse, M. Rabec-Le Gloahec, I. Matsushima, C. Bauche-Arnoult, A. Bachelier, and J. Bauche, "X-ray emission of a xenon gas jet plasma diagnosed with thomson scattering," *Phys. Rev. E* **65**, 046418 (2002).
- ⁸T. Pütterich, R. Neu, R. Dux, A. D. Whiteford, M. G. O'Mullane, and the ASDEX Upgrade Team, "Modelling of measured tungsten spectra from ASDEX upgrade and predictions for ITER," *Plasma Phys. Control. Fusion* **50**, 085016 (2008).
- ⁹Y. Ralchenko, "Collisional-Radiative Modeling for Highly-Charged ions of Tungsten," *Plasma*

This is the author's peer reviewed, accepted manuscript. However, the online version of record will be different from this version once it has been copyedited and typeset.

PLEASE CITE THIS ARTICLE AS DOI: 10.1063/1.50160913

- and Fusion Research **8**, 2503024 (2013).
- ¹⁰R. Radtke, C. Biedermann, J.L. Schwob, P. Mandelbaum, and R. Doron, "Line and band emission from tungsten ions with charge 21+ to 45+ in the 45-70 angstrom range," Phys. Rev. A **64**, 012720 (2001).
- ¹¹S.B. Utter, P. Beiersdorfer, and E. Träbert, "Electron beam ion-trap spectra of tungsten in the EUV," Can. J. Phys. **80**, 1503 (2002).
- ¹²Yu. Ralchenko, J. Reader, J.M. Pomeroy, J.N. Tan, and J.D. Gillaspay, "Spectra of W³⁹⁺-W⁴⁷⁺ in the 12-20 nm region observed with an EBIT light source," J. Phys. B: At. Mol. Opt. Phys. **40**, 3861 (2007).
- ¹³C. Biedermann, R. Radtke, R. Seidel, and T. Pütterich, "Spectroscopy of highly charged tungsten ions relevant to fusion plasmas," Physica Scripta **T134**, 014026 (2009).
- ¹⁴D. Post, R. Jensen, C. Tarter, W. Grasberger, and W. Lokke, "Steady-state radiative cooling rates for low-density, high-temperature plasmas," Atom. Data Nucl. Data Tables **20**, 397 (1977).
- ¹⁵K. Asmussen, K. Fournier, J. Laming, R. Neu, J.F. Seely, R. Dux, W. Engelhardt, J.C. Fuchs, and ASDEX Upgrade Team, "Spectroscopic investigations of tungsten in the EUV region and the determination of its concentration in tokamaks," Nucl. Fusion **38**, 967 (1998).
- ¹⁶S.D. Loch, J.A. Ludlow, M.S. Pindzola, A.D. Whiteford, and D.C. Griffin, "Electron-impact ionization of atomic ions in the W isonuclear sequence," Phys. Rev. A **72**, 052716 (2005).
- ¹⁷OPEN-ADAS Project 1995-2016 <http://open.adas.ac.uk>.
- ¹⁸S.B. Hansen, in *Modern methods in Collisional-Radiative modeling of plasmas*, edited by Y. Ralchenko (Springer, 2016).
- ¹⁹O. Peyrusse, C. Bauche-Arnoult, and J. Bauche, "Calculation of the charge state distribution of a highly ionized coronal Au plasma," J. Phys. B: At. Mol. Opt. Phys. **38**, L137 (2005).
- ²⁰J. Bauche, C. Bauche-Arnoult, and K.B. Fournier, "Model for computing superconfiguration temperatures in non-local-thermodynamic-equilibrium hot plasmas," Phys. Rev. E **69**, 026403 (2004).
- ²¹O. Peyrusse, C. Bauche-Arnoult, and J. Bauche, "Effective superconfiguration temperature and the radiative properties of non-local thermodynamical equilibrium hot dense plasma," Phys. Plasmas **12**, 063302 (2005).
- ²²A. Herman, "Empirically adjusted and consistent set of EHT valence orbital parameters for all elements of the periodic table," Modelling Simul. Mater Sci. Eng. **12**, 21 (2004).

This is the author's peer reviewed, accepted manuscript. However, the online version of record will be different from this version once it has been copyedited and typeset.

PLEASE CITE THIS ARTICLE AS DOI: 10.1063/5.0160913

- ²³O. Peyrusse, "Atomic configuration averages and non-local thermodynamical equilibrium plasma spectroscopy calculations," *J. Phys. B* **32**, 683 (1999).
- ²⁴J. Colgan, C.J. Fontes, H. Zhang, and J. Abdallah Jr, "Collisional-radiative modeling of tungsten at temperatures of 1200?2400 eV," *Atoms* **3**, 76 (2015).
- ²⁵J. Bauche, C. Bauche-Arnoult, and M. Klapisch, "Transition arrays in the spectra of ionized atoms," *Adv. At. Mol. Phys.* **23**, 131 (1988).
- ²⁶J. Bauche and C. Bauche-Arnoult, "Statistical properties of atomic spectra," *Computer Physics Reports* **12**, 3 (1990).
- ²⁷T. Blenski, A. Grimaldi, and F. Perrot, "Hartree-Fock statistical approach to atoms and photoabsorption in plasmas," *Phys. Rev. E* **55**, R4889 (1997).
- ²⁸J. Bauche, C. Bauche-Arnoult, and M. Klapisch, "Breakdown of jj coupling in spin-orbit-split atomic transition arrays," *J. Phys. B: At. Mol. Opt. Phys.* **24**, 1 (1991).
- ²⁹A. Bar-Shalom, J. Oreg, and W.H. Goldstein, "Configuration interaction in LTE spectra of Heavy Elements," *J. Quant. Spectrosc. Rad. Transfer* **51**, 27 (1994).
- ³⁰F. Gilleron, J. Bauche, and C. Bauche-Arnoult, "A statistical approach for simulating detailed-line spectra," *J. Phys. B: At. Mol. Opt. Phys.* **40**, 3057 (2007).
- ³¹R.C. Isler, R.V. Neidigh, and R.D. Cowan, "Tungsten radiation from tokamak-produced plasmas," *Phys. Lett. A* **63**, 295 (1977).
- ³²M. Finkenthal, L.K. Huang, S. Lippmann, H.W. Moos, P. Mandelbaum, J.L. Schwob, M. Klapisch, and Text Group, "Soft x-ray bands of highly ionized tungsten, gold and lead emitted by the TEXT tokamak plasma," *Phys. Lett. A* **127**, 255 (1988).
- ³³Y. Liu, S. Morita, X. Huang, T. Oishi, M. Goto, and H. Zhang, "Component investigation of ionization stages on tungsten unresolved transition array spectra for plasma diagnostics based on space-resolved extreme-ultra violet spectroscopy in large helical device," *J. App. Phys.* **122**, 233301 (2017).
- ³⁴R. Guirlet, C. Desgranges, J.L. Schwob, P. Mandelbaum, M. Y. Boumendjel, and the WEST Team, "Extreme UV spectroscopy measurements and analysis for tungsten density studies in the west tokamak," *Plasma Phys. Control. Fusion* **64**, 105024 (2022).
- ³⁵J.L. Schwob, A. W. Wouters, S. Suckewer, and M. Finkenthal, "High-resolution duo-multichannel soft x-ray spectrometer for tokamak plasma diagnostics," *Review of scientific instruments* **58**, 1601 (1987).

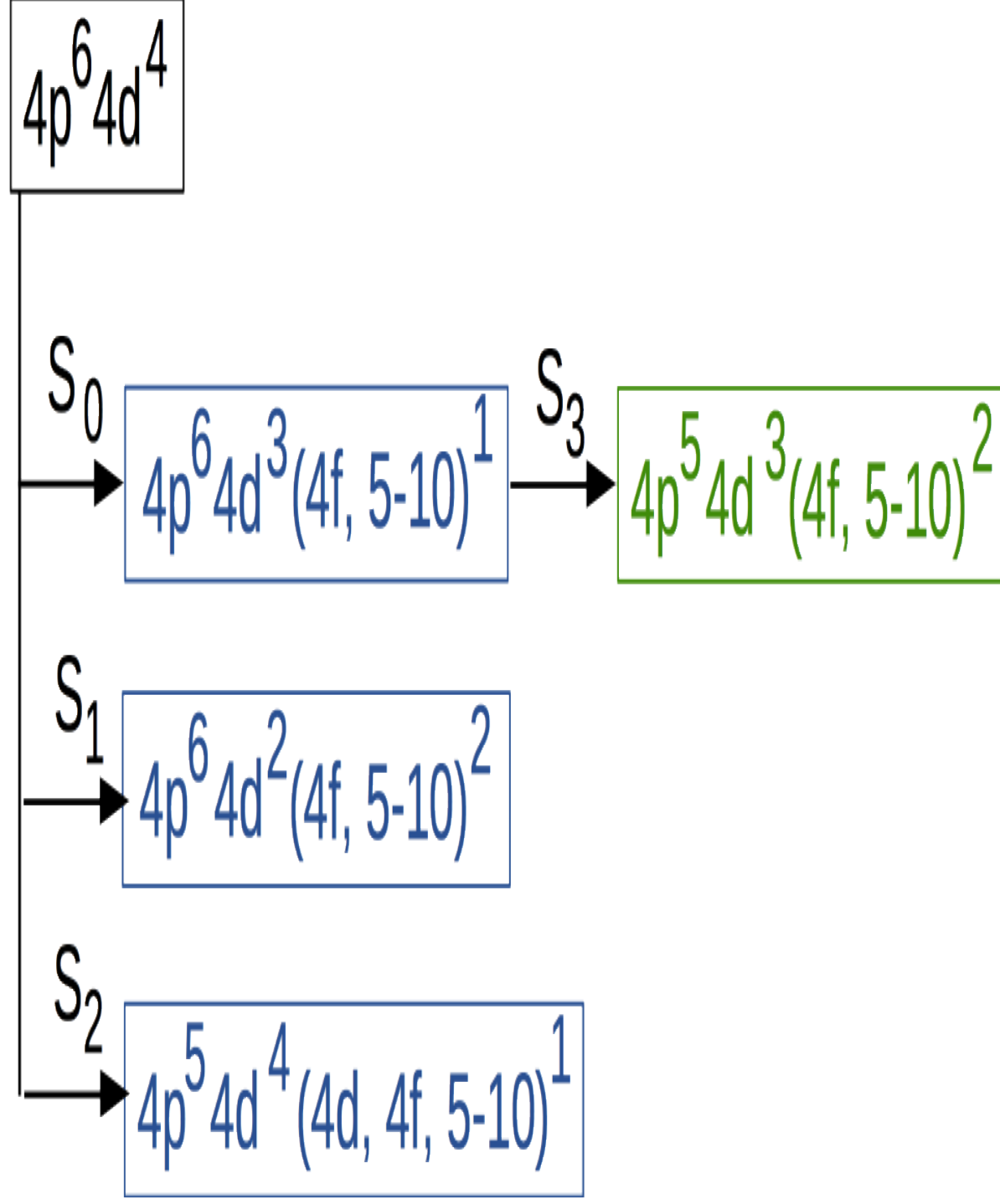
This is the author's peer reviewed, accepted manuscript. However, the online version of record will be different from this version once it has been copyedited and typeset.

PLEASE CITE THIS ARTICLE AS DOI: 10.1063/1.50160913

- ³⁶R. Guirlet, J.L. Schwob, O. Meyer, and S. Vartanian, "Absolute sensitivity calibration of an extreme ultraviolet spectrometer for tokamak measurements," *Journal of Instrumentation* **12**, P01006 (2017).
- ³⁷R.J. Groebner, D.R. Baker, K.H. Burrell, T.N. Carlstrom, J.R. Ferron, P. Gohil, L.L. Lao, T.H. Osborne, D.M. Thomas, W.P. West, J.A. Boedo, R.A. Moyer, G.R. McKee, R.D. Deranian, E.J. Doyle, C.L. Rettig, T.L. Rhodes, and J.C. Rost, "Progress in quantifying the edge physics of the H mode regime in DIII-D," *Nuclear Fusion* **41**, 1789 (2001).
- ³⁸J.L. Ségui, D. Molina, G. Giruzzi, M. Goniche, G. Huysmans, P. Maget, M. Ottaviani, and The Tore Supra Team, "An upgraded 32-channel heterodyne electron cyclotron emission radiometer on Tore Supra," *Review of scientific instruments* **76**, 123501 (2005).
- ³⁹R. Mazevet and J. Abdallah Jr, "Mixed UTA and detailed line treatment for mid-Z opacity and spectral calculations," *J. Phys. B: At. Mol. Opt. Phys.* **39**, 3419 (2006).

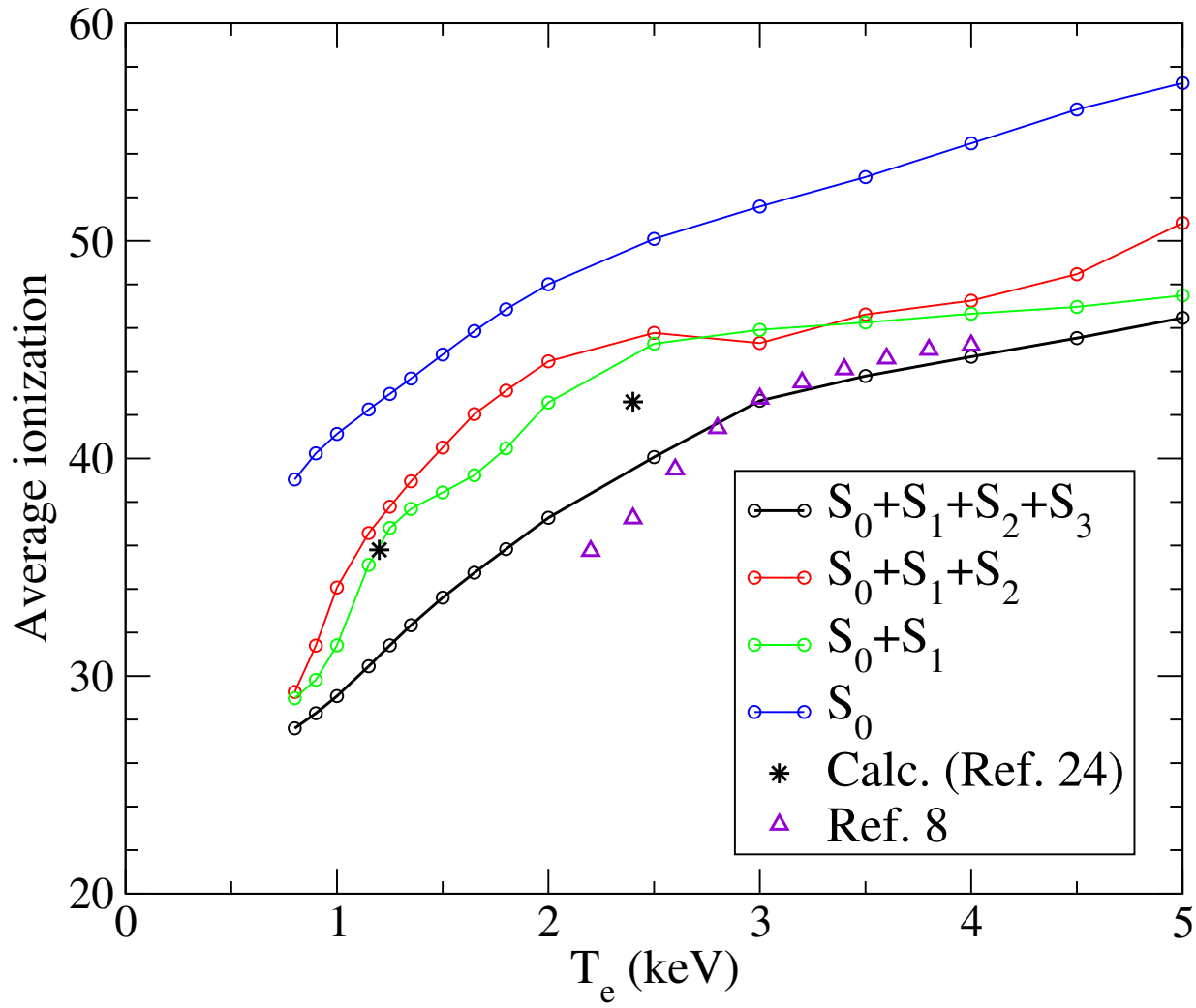
This is the author's peer reviewed, accepted manuscript. However, the online version of record will be different from this version once it has been copyedited and typeset.

PLEASE CITE THIS ARTICLE AS DOI: 10.1063/5.0160913



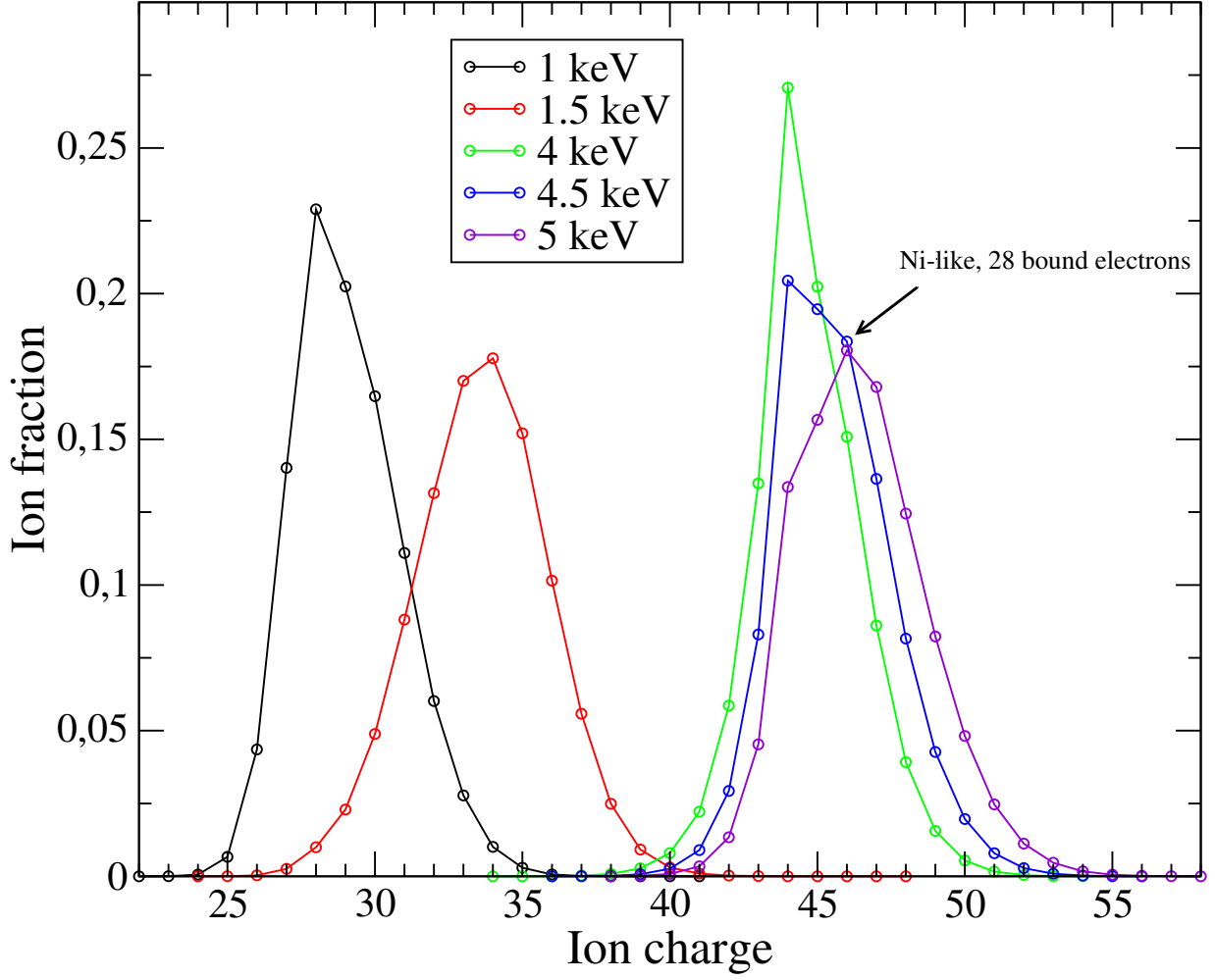
This is the author's peer reviewed, accepted manuscript. However, the online version of record will be different from this version once it has been copyedited and typeset.

PLEASE CITE THIS ARTICLE AS DOI: 10.1063/5.0160913



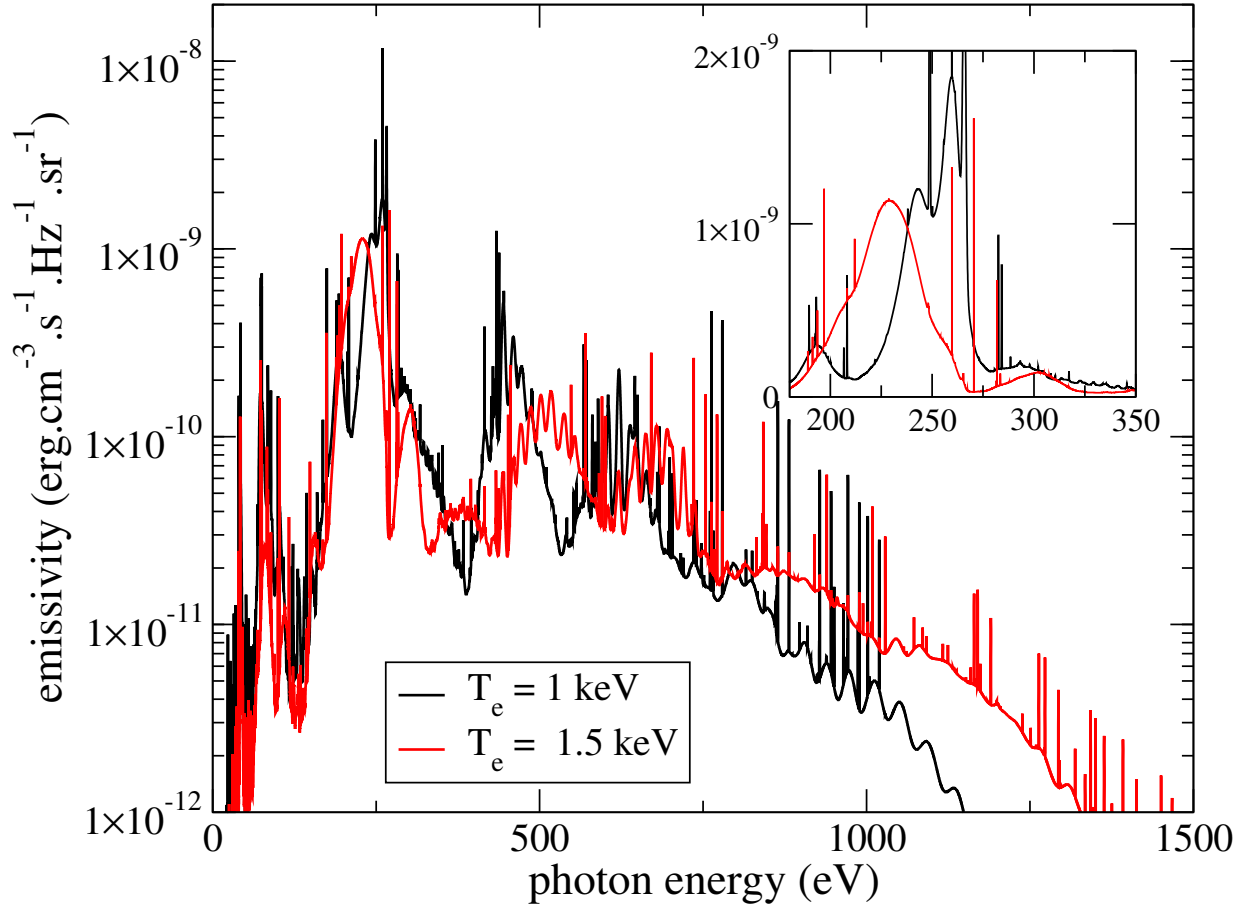
This is the author's peer reviewed, accepted manuscript. However, the online version of record will be different from this version once it has been copyedited and typeset.

PLEASE CITE THIS ARTICLE AS DOI: 10.1063/5.0160913



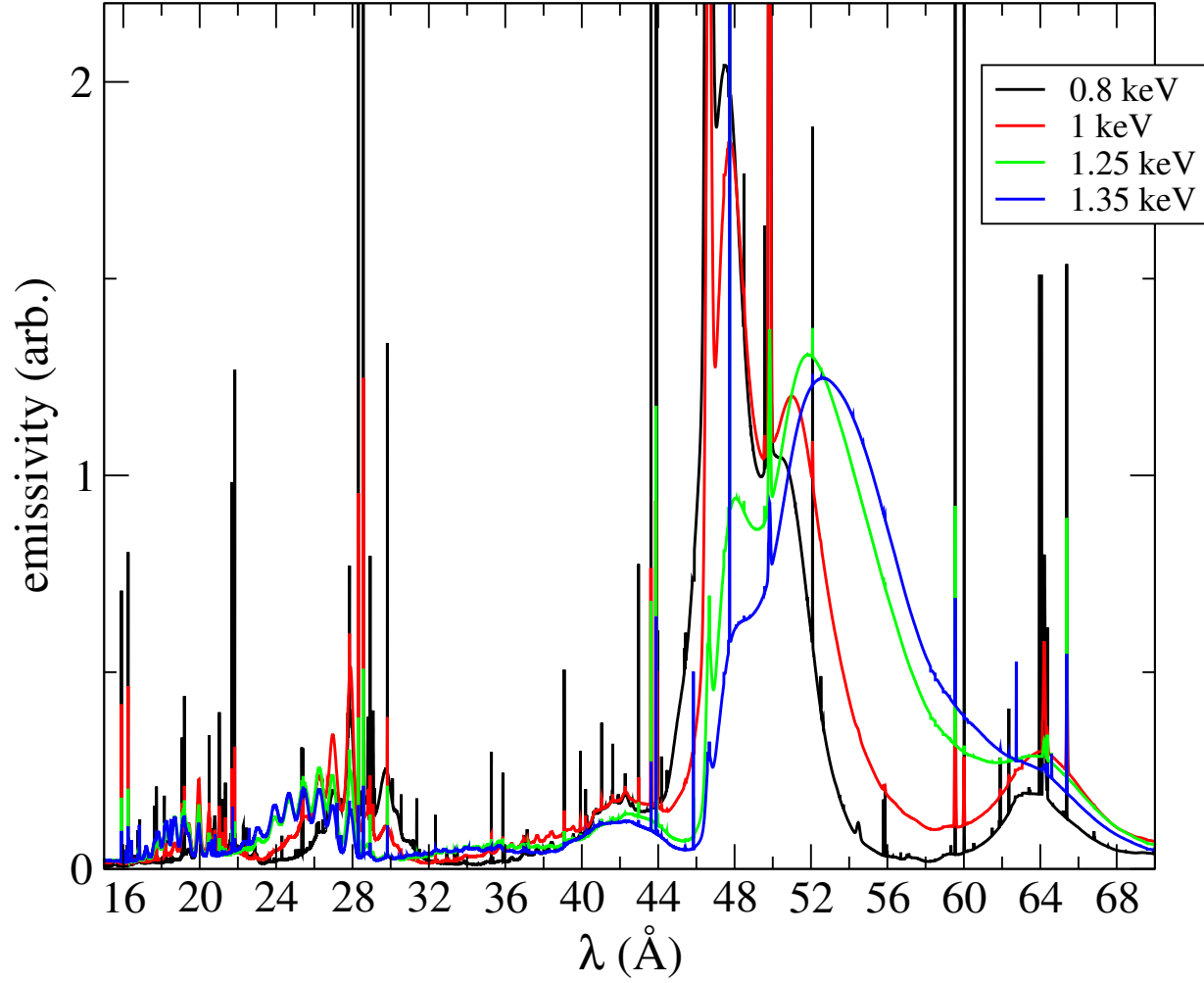
This is the author's peer reviewed, accepted manuscript. However, the online version of record will be different from this version once it has been copyedited and typeset.

PLEASE CITE THIS ARTICLE AS DOI: 10.1063/5.0160913



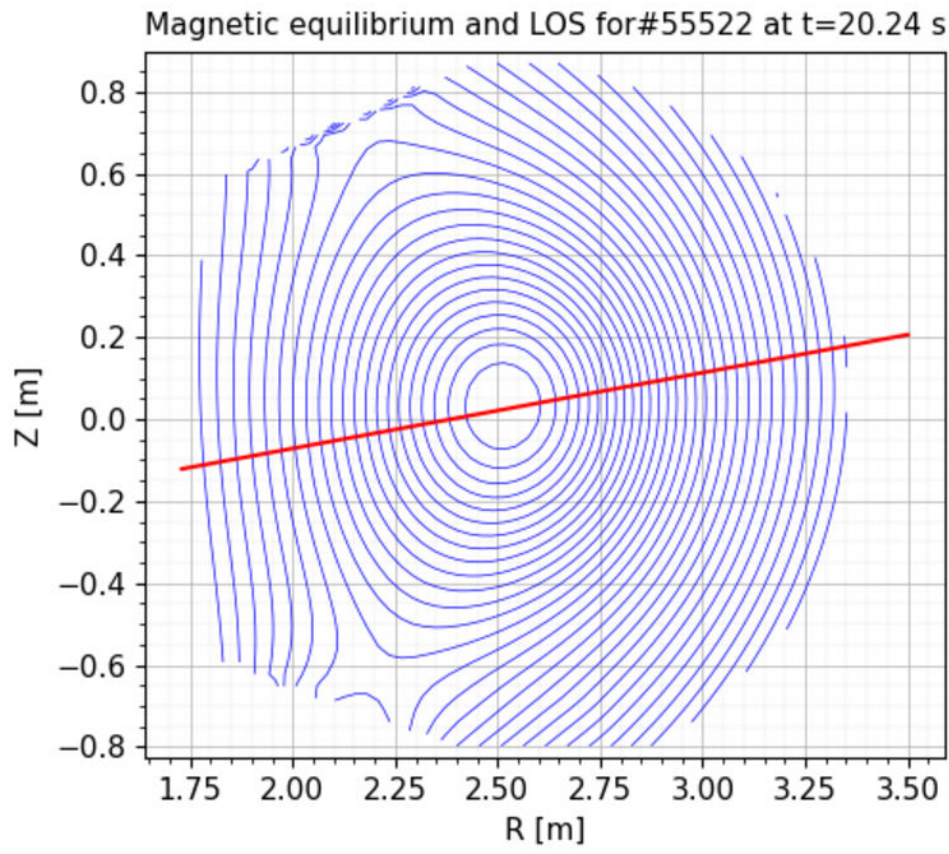
This is the author's peer reviewed, accepted manuscript. However, the online version of record will be different from this version once it has been copyedited and typeset.

PLEASE CITE THIS ARTICLE AS DOI: 10.1063/5.0160913



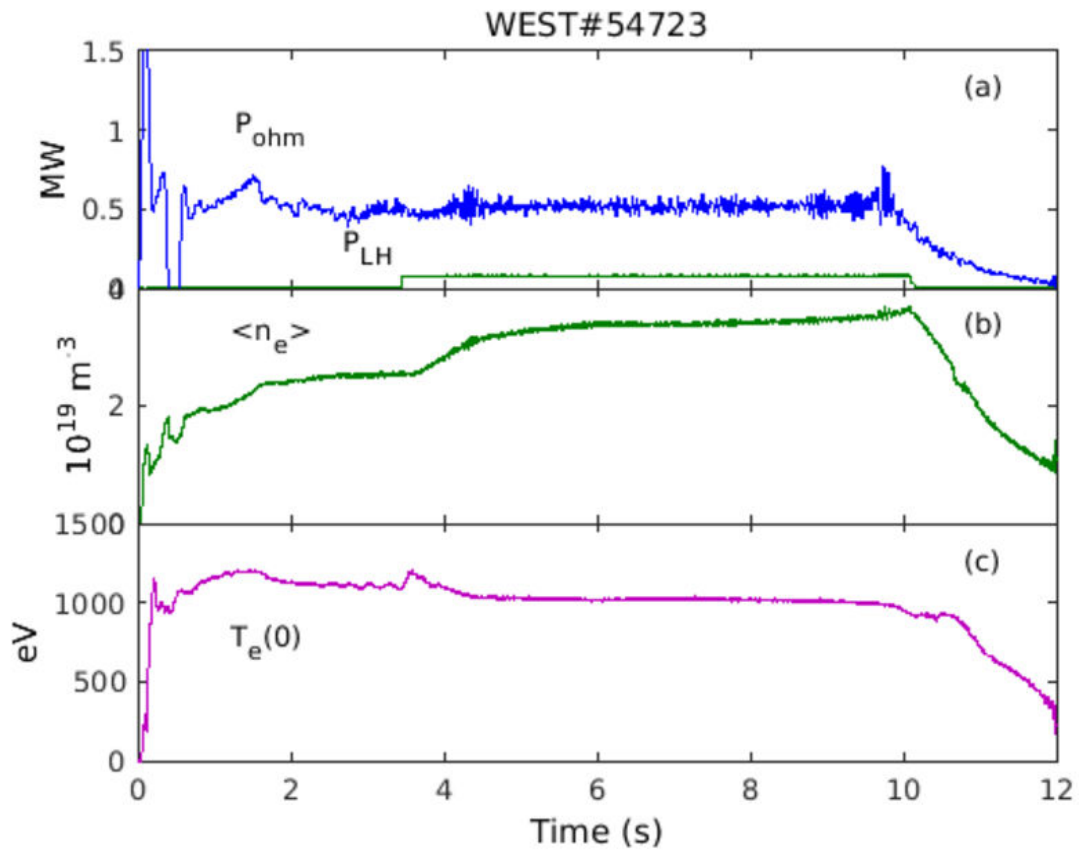
This is the author's peer reviewed, accepted manuscript. However, the online version of record will be different from this version once it has been copyedited and typeset.

PLEASE CITE THIS ARTICLE AS DOI: 10.1063/5.0160913



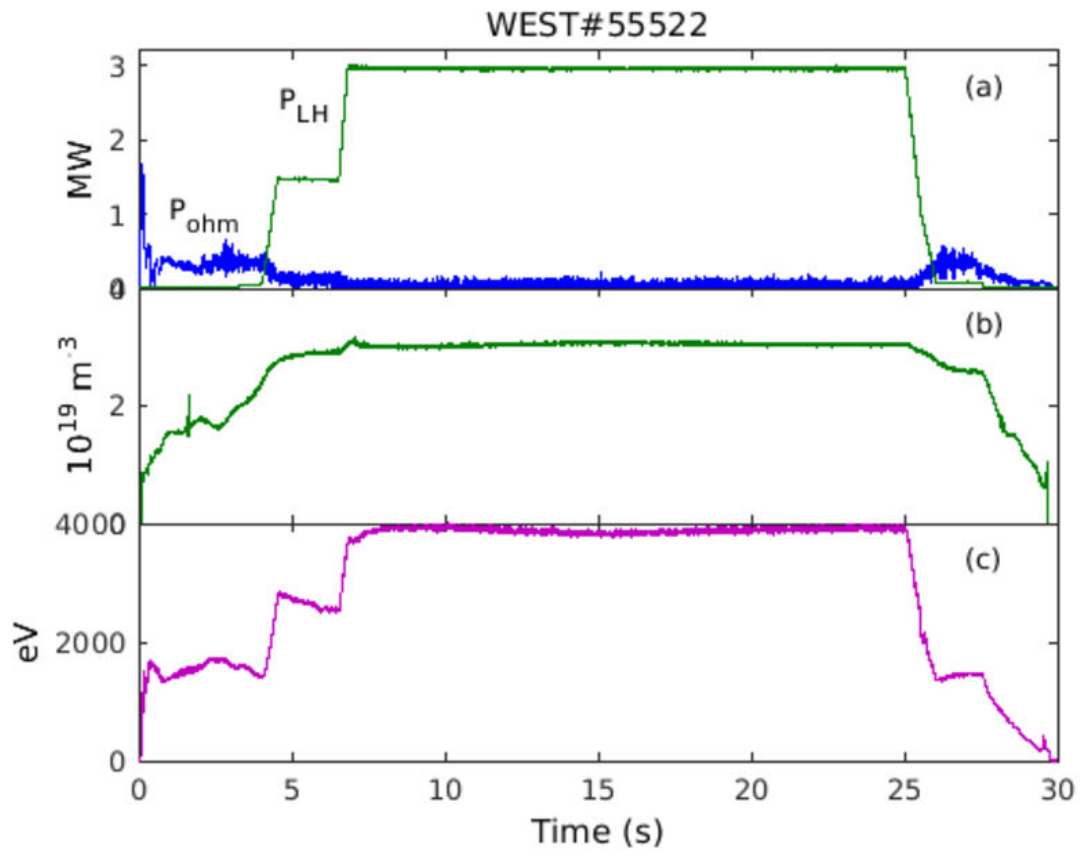
This is the author's peer reviewed, accepted manuscript. However, the online version of record will be different from this version once it has been copyedited and typeset.

PLEASE CITE THIS ARTICLE AS DOI: 10.1063/1.50160913



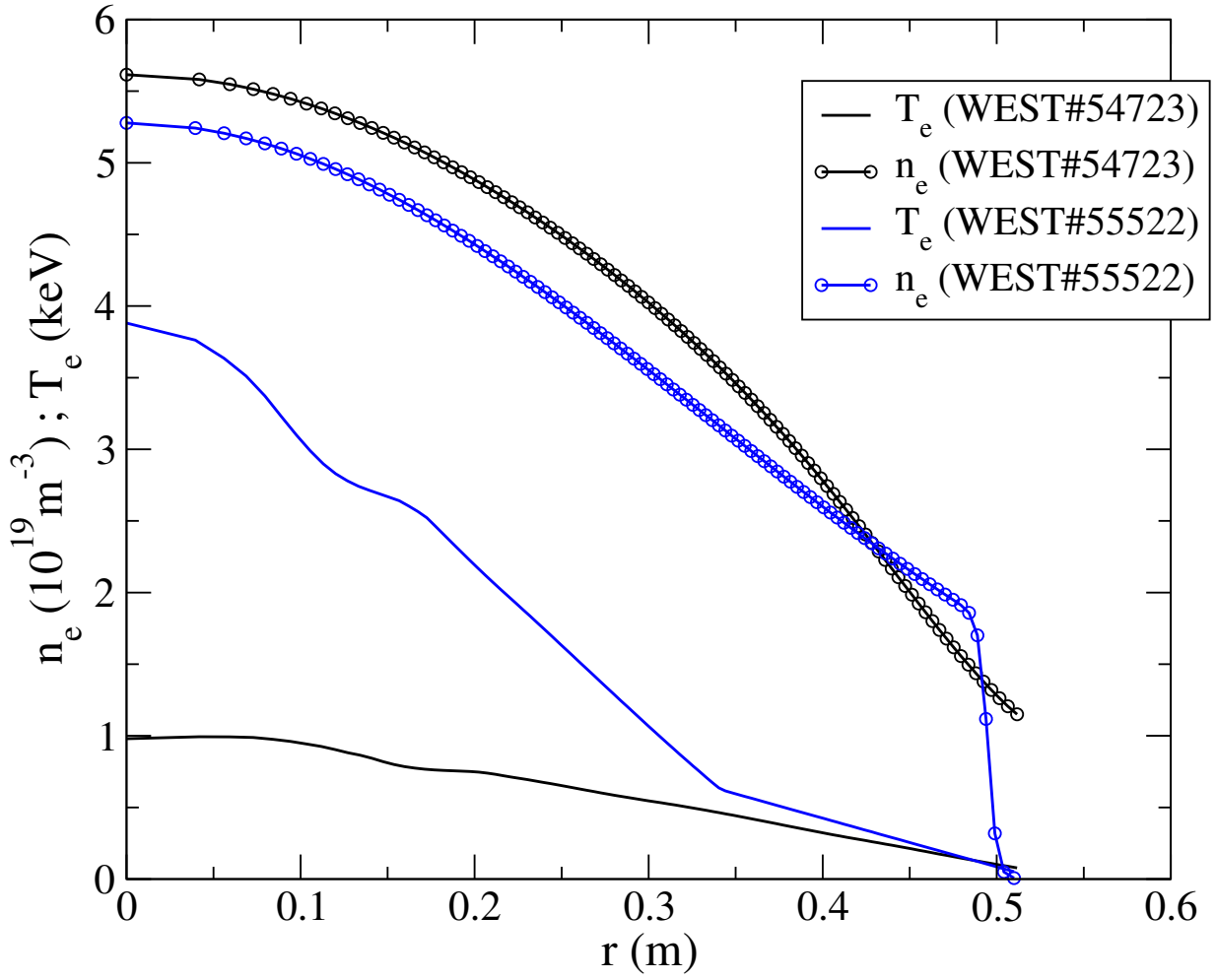
This is the author's peer reviewed, accepted manuscript. However, the online version of record will be different from this version once it has been copyedited and typeset.

PLEASE CITE THIS ARTICLE AS DOI: 10.1063/5.0160913



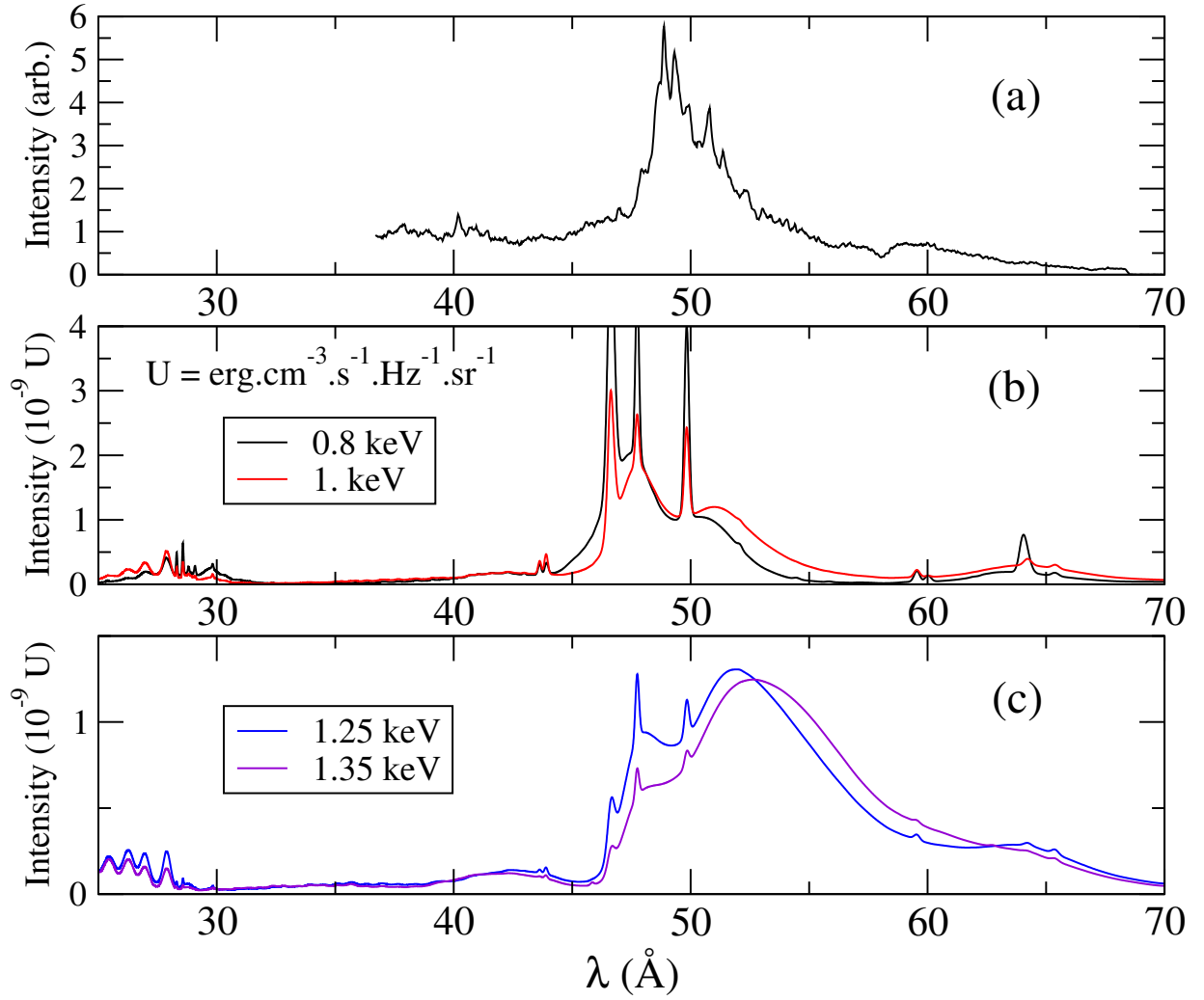
This is the author's peer reviewed, accepted manuscript. However, the online version of record will be different from this version once it has been copyedited and typeset.

PLEASE CITE THIS ARTICLE AS DOI: 10.1063/5.0160913



This is the author's peer reviewed, accepted manuscript. However, the online version of record will be different from this version once it has been copyedited and typeset.

PLEASE CITE THIS ARTICLE AS DOI: 10.1063/5.0160913



This is the author's peer reviewed, accepted manuscript. However, the online version of record will be different from this version once it has been copyedited and typeset.

PLEASE CITE THIS ARTICLE AS DOI: 10.1063/5.0160913

